

Experimental verification of numerical simulations of cryosurgery with application to computerized planning

Michael R Rossi and Yoed Rabin¹

Biothermal Technology Laboratory, Department of Mechanical Engineering,
Carnegie Mellon University, Pittsburgh, PA 15213, USA

E-mail: rabin@cmu.edu

Received 6 March 2007, in final form 4 May 2007

Published 3 July 2007

Online at stacks.iop.org/PMB/52/4553

Abstract

As a part of an ongoing effort to develop computerized planning tools for cryosurgery, an experimental study has been conducted to verify a recently developed numerical technique for bioheat transfer simulations. Experiments were performed on gelatin solution as a phantom material, using proprietary liquid-nitrogen cryoprobes. Urethral warming was simulated with the application of a cryoheater, which is a proprietary temperature-controlled electrical heater. The experimental design was aimed at creating a 2D heat transfer problem. Analysis of experimental results was based on reconstruction of the frozen region from video recordings, using a region-growing segmentation algorithm. Results of this study show an average disagreement of 2.9% in the size of the frozen region, between experimental data and numerical simulation of the same experiment, which validates both the recently developed algorithm for numerical simulations and the newly developed algorithm for segmentation from video recordings.

(Some figures in this article are in colour only in the electronic version)

1. Introduction

Cryosurgery is the destruction of undesired biological tissues by freezing (Cooper and Lee 1961). Modern cryosurgery is frequently performed as a minimally-invasive procedure, in which a number of cryoprobes (up to about a dozen) are inserted into the target area to be treated (Gage 1992). While there is an extensive body of literature on the factors affecting cryosurgery success (with the lethal temperature threshold of $-45\text{ }^{\circ}\text{C}$ as possibly the most commonly accepted factor in recent years (Gage and Baust 1998)), it is the match between

¹ Author to whom any correspondence should be addressed.

the frozen region contour and the outer surface of the target region which is currently used for cryosurgery control. This match is evaluated with the application of an imaging device such as ultrasound or MRI (Onik *et al* 1993, 1985, Rubinsky *et al* 1993, Schulz *et al* 2004). The cryoprobe layout is a key factor for achieving the highest quality of that match and, therefore, for the success of cryosurgery.

To date, cryoprobe localization is an art held by the cryosurgeon, based on the surgeon's own experience and accepted practices. Currently, the means for determining the optimal locations or thermal history for the cryoprobes are limited. Suboptimal cryoprobe localization may leave areas in the target region untreated, may lead to cryoinjury of healthy surrounding tissues, may require an unnecessarily large number of cryoprobes, may increase the duration of the surgical procedure, and may increase the likelihood of post cryosurgery complications, all of which affect the quality and cost of the medical treatment. Computerized planning tools would help to alleviate these difficulties, which is the subject matter of this ongoing research program at the Biothermal Technology Laboratory (Lung *et al* 2004, Rabin *et al* 2004, Rabin and Stahovich 2003, Rossi *et al* 2007, Tanaka *et al* 2006, 2007).

Since temperature can be measured only at discrete points in the target region, simulation of heat transfer is an extremely useful tool in developing and improving cryosurgical techniques (Baissalov *et al* 2001, Diller 1992, Keanini and Rubinsky 1992, Turk *et al* 1999). Here, heat transfer simulations can be calibrated with temperature measurements in the target tissue for the purpose of parametric estimation of tissue properties (Rabin *et al* 1996), assist in evaluating the certainty in temperature measurements (Rabin 1998), and augment imaging in real time by identifying specific temperature thresholds within the frozen region (Gilbert *et al* 1997). However, the quality of those simulations depends on the certainty in value of the thermophysical properties of the tissue (Rabin 2003), and the accuracy of the numerical scheme used.

Recently, a new 3D numerical scheme has been presented, which has been developed for short runtime of cryosurgery simulations (Rossi *et al* 2007), in order to make several prototypes of computerized planning tools clinically relevant (Lung *et al* 2004, Rabin *et al* 2004, Tanaka *et al* 2006). The current study is focused on experimental verification of that numerical scheme. A new experimental apparatus for verification of computerized planning in 2D is presented, along with a technique for analysis of the frozen region shape from video recording, and a comparison of experimental data with numerical simulation results on representative cryoprobe layouts. Consistent with cryosurgery practice, where the freezing front is monitored with imaging devices, the current study focuses on the ability to trace the freezing front with the proposed numerical scheme.

2. Experimental setup

A schematic illustration of the experimental setup is shown in figure 1. The experimental setup is designed for 2D cryosurgery simulation on a gelatin solution (1.6% by weight) as a phantom material, where the 2D setup is representative of a prostate cross-section. The thermophysical properties of pure water are close to those of soft tissues, as listed in table 1, and the gelatin is added to prevent convective heat transfer in the domain. In order to accentuate the contrast between the frozen and unfrozen regions in the gelatin, blue food dye was added at a concentration of about 0.4 ml liter⁻¹.

A proprietary cryodevice is used in the current study, which is a modification of an earlier device, based on liquid-nitrogen cooling (Rabin *et al* 1997, 2000). The new experimental setup uses the same cryogen control and supply system presented earlier (Rabin *et al* 1997, 2000), with newly designed cryoprobes, as illustrated in figure 2. The new cryoprobes are similar to

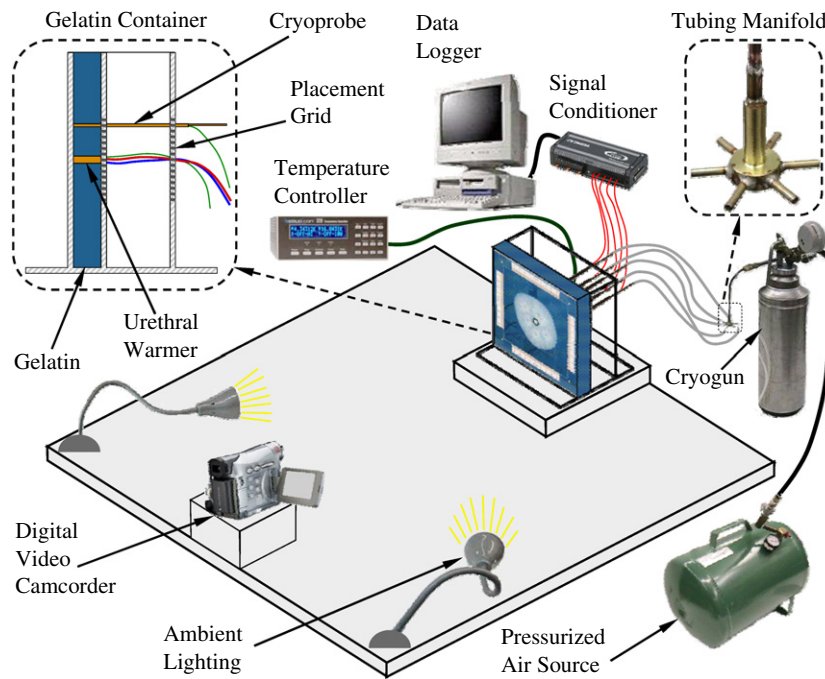


Figure 1. Schematic illustration of the experimental setup.

Table 1. Thermophysical properties of pure water and typical thermophysical properties of biological tissues used, where T is in degree K (Rabin and Stahovich 2003, Rabin *et al* 2004, Holman 2002).

Property	Water		Biological tissues	
Thermal conductivity, k ($\text{W m}^{-1} \text{K}^{-1}$)	0.58	$273 < T$	0.50	$273 < T$
	$2135 \times T^{-1.235}$	$T < 273$	$16.0 - 0.0567 \times T$	$251 < T < 273$
			$1005 \times T^{-1.15}$	$T < 251$
Volumetric specific heat, C ($\text{MJ m}^{-3} \text{K}^{-1}$)	4.20	$275 < T$	3.60	$273 < T$
	86.6	$271 < T < 275$	15.4	$251 < T < 273$
	$0.0078 \times T$	$T < 271$	$0.00398 \times T$	$T < 251$
Latent heat, L (MJ m^{-3})	333.7		300	
Blood perfusion heating effect, $w_b C_b$ ($\text{kW m}^{-3} \text{K}^{-1}$)	0		0–40	

the original cryoprobes invented by Cooper and Lee (1961), with the exception of an off-center internal tube, and an embedded T-type thermocouple in the outer wall. The tubes are made of copper; the external diameter of the inner and outer tubes are 1.6 mm and 3.2 mm, respectively; the lengths of the inner and outer tubes are 160 mm and 110 mm, respectively; and the wall thickness of both is 0.4 mm. Up to six cryoprobes are connected to the liquid-nitrogen supply system with 1.6 mm ID Tygon tubing and a brass manifold. Experiments were conducted in the current study subject to relatively low pressure in the liquid-nitrogen supply system—below 20 psi. Simultaneous operation of six cryoprobes under this pressure led to a cooling rate of about $33^\circ\text{C min}^{-1}$ in the first three minutes of operation, and a minimum operation temperature

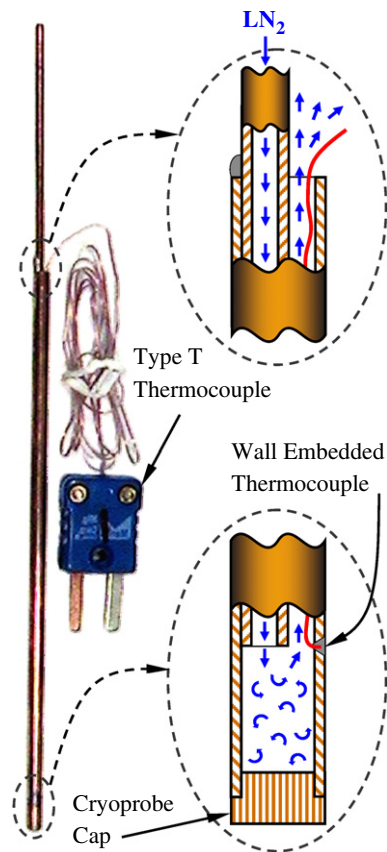


Figure 2. An image of a cryoprobe, including two enlarged illustrations displaying the cryoprobe design and functionality.

of about $-110\text{ }^{\circ}\text{C}$. Increasing the pressure would dramatically increase the cooling rate, while decreasing the minimum temperature towards the liquid-nitrogen boiling temperature of $-196\text{ }^{\circ}\text{C}$ (Rabin *et al* 1997). However, such an increase in pressure would result in a significant decrease in the thermal efficiency of the system (Rabin *et al* 1997). Given the target region size and the 2D nature of the heat transfer process, a pressure upper limit of 20 psi was deemed adequate.

Urethral warming in the current setup is simulated with a cryoheater (Rabin *et al* 1999, Rabin and Stahovich 2003). The cryoheater is a self-controlled electric heater, embedded either in a hypodermic needle or a catheter. Embedded in a catheter, the cryoheater is an alternative to the common urethral warmer, made of a double-pipe water heat exchanger. The cryoheater in the current study is placed inside a 7 mm OD thin-wall brass tube, and a T-type thermocouple is embedded in the wall of the cryoheater, for control purposes. A cryogenic controller and a power supply in one unit are used to maintain the temperature of the urethral warmer constant throughout the experiment (Cryocon, Model 32). The output of the power supplier is 50 V DC and the resistance of the cryoheater is $90\ \Omega$, which leads to a maximum heating power of 26 W, or $1.0\ \text{W mm}^{-1}$ for the specific exposure length of cryoheater to gelatin. This power rate is found to be adequate for urethral warming by means of a cryoheater.

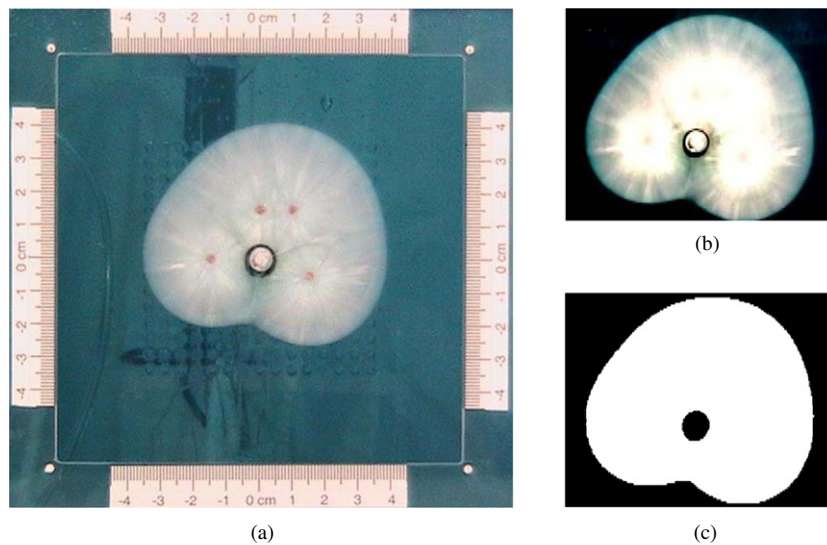


Figure 3. Segmentation of the experimental image: (a) original experimental bitmap image captured from the video, (b) frozen region after maximizing contrast, and (c) segmented frozen region.

With reference to figure 1, the gelatin container is made of 5 mm thick Plexiglas plates, with a gelatin chamber of 25 mm \times 200 mm \times 200 mm. A grid of 15 \times 15 holes with 5 mm intervals is drilled in one side of the container to accommodate the cryoprobes (3.2 mm in diameter). A 7 mm in diameter hole is drilled at the center of the grid to accommodate the cryoheater. An additional plate, having an identical grid, is connected to the container base at a distance of 65 mm, to ensure cryoprobe alignment. Uncertainty in cryoprobe location is estimated as 0.25 mm.

Temperature data from the cryoprobes and the cryoheater are collected through a USB data acquisition system (Omega, OMB-DAQ-56) and are computer-recorded. Experiments are also video-recorded (Canon ZR300 Mini DV camcorder); the camcorder is placed on a special stage, approximately 0.7 m from the container. Two 40 W light sources are used to ensure appropriate illumination for video recording. Four reference scales are placed around the perimeter of the front of the container, as displayed in figure 3(a). Additionally, four white dots are added to the corners of the viewed surface of the container, for registration purposes.

3. Frozen region reconstruction

For each experiment in the current study, one image (snap-shot) per second is taken from video recording, figure 3(a), for the purpose of frozen region reconstruction. The contrast of the image is enhanced with Adobe Photoshop 7.0, as displayed in figure 3(b). Using MATLAB, the image is then converted from a true color RGB image to an 8 bit grayscale image, with intensities ranging from 0 (black) to 255 (white). In order to further sharpen the edge between the frozen region and the surrounding unfrozen domain, the MATLAB filter 'unsharp' is used, with default MATLAB parameters. Because of the high contrast level achieved, a relatively simple region-growing segmentation technique (Chang and Li 1994, Pohle and Toennies 2001) is then applied, as described below.

For the current study, the segmentation of the frozen region begins at seed points, which are the center of the cryoprobe locations on the first image. Each pixel surrounding the seed is evaluated with respect to its level of intensity, α , and its proximity to previously added pixels, β , in order to determine whether the pixel represents a unit area in the frozen region or the unfrozen region. For each pixel outside the segmented domain, the β value is determined by summing up all the pixels within a 4 pixel radius which are already defined as parts of the frozen region. These neighboring pixels are inversely weighted with respect to their distance from the pixel under consideration, and the weights are normalized so that β ranges between 0 and 1. Based on calibration with manual segmentations, a pixel is considered representative of the frozen region if at least one of the following criteria is satisfied: (1) $0.7 < \beta$; (2) $0.5 < \beta$ and $30 < \alpha$; (3) $0.3 < \beta$ and $50 < \alpha$. This process is repeated until no additional pixels can be identified as representative of the frozen region.

After the segmented region has grown to its maximum size, a dilation transformation is performed. Dilation is a mathematical-morphological operation (Serra 1982), which enlarges the segmented image by adding pixels to its boundary, thus filling small holes and gaps. For the current study, each pixel along the boundary of the segmented image is given a score based on its neighbors, within a 3×3 grid centered around that pixel. The score is the sum of the neighbor values, where a side neighbor representing a frozen region gets a value of 2, a corner neighbor representing a frozen region gets a value of 1, and a neighbor representing the unfrozen region gets a 0 value. A pixel is added to the frozen region if its score is greater than 5. Figure 3(c) displays the results for the image displayed in figure 3(b) upon completion of the segmentation and dilation. This is the final reconstructed experimental domain used for comparison with a simulated result.

After completion of reconstruction, an erosion transformation (Serra 1982) is performed to shrink the segmented region, so that it can then be used as a seed for the subsequent image segmentation (to reduce computational cost). Here, a pixel is removed from the frozen region if any of its eight neighbors are already outside the domain. The erosion transformation is performed sequentially three times. This process is repeated for all of the snap-shots taken from the recorded video.

By comparison with manual segmentation, uncertainty in the automatic reconstruction technique presented above is estimated as 2% of the frozen region size, which corresponds to 0.25 mm uncertainty in identification of the freezing front location.

4. Numerical solution of bioheat transfer

For the purpose of computerized planning, it is assumed in previous studies (Lung *et al* 2004, Rabin *et al* 2004, Rabin and Shitzer 1998, Rossi *et al* 2007, Tanaka *et al* 2006) that the classical bioheat equation (Pennes 1948) can be used to model heat transfer during cryosurgery of the prostate:

$$C \frac{\partial T}{\partial t} = \nabla \cdot (k \nabla T) + \dot{w}_b C_b (T_b - T) + \dot{q}_{\text{met}} \quad (1)$$

where C is the volumetric specific heat of the tissue, T is the temperature, t is the time, k is the thermal conductivity of the tissue, \dot{w}_b is the blood perfusion volumetric flow rate per unit volume of tissue, C_b is the volumetric specific heat of the blood, T_b is the blood temperature entering the thermally treated area and \dot{q}_{met} is the metabolic heat generation.

A numerical technique has been proposed to solve equation (1), using a finite difference scheme (Rabin and Shitzer 1998), and is presented here in brief for the completeness of presentation. For this purpose, equation (1) is rewritten in a finite difference form, and

reorganized to yield the incremental change in the spatial temperature distribution:

$$T_{i,j,k}^{p+1} = \frac{\Delta t}{\Delta V_{i,j,k}[C_{i,j,k} + (\dot{w}_b C_b)_{i,j,k} \Delta t]} \sum_{l,m,n} \frac{T_{l,m,n}^p - T_{i,j,k}^p}{R_{l,m,n-i,j,k}} + \frac{\Delta t[(\dot{w}_b C_b)_{i,j,k} T_b + (\dot{q}_{\text{met}})_{i,j,k}] + C_{i,j,k} T_{i,j,k}^p}{C_{i,j,k} + (\dot{w}_b C_b)_{i,j,k} \Delta t} \quad (2)$$

where i, j, k are spatial indices of the temperature field, l, m, n are spatial indices of the neighboring grid points, p is a time index, ΔV is an element volume associated with a grid point, Δt is a time interval, and R is the thermal resistance to heat transfer by conduction between node i, j, k and its neighbor l, m, n . Equation (2) is rather general and independent of the coordinate system and the number of dimensions of the problem. For a regular Cartesian geometry, the thermal resistance to heat conduction can be presented as:

$$R_{l,m,n-i,j,k} = \left[\frac{\Delta \eta}{2kA} \right]_{l,m,n} + \left[\frac{\Delta \eta}{2kA} \right]_{i,j,k} \quad (3)$$

where the length $\Delta \eta$ is the space interval in the direction of interest, and A is the representative cross-sectional area perpendicular to the direction of heat flow.

More recently, the above numerical scheme has been optimized for short runtime (Rossi *et al* 2007), using a variable grid scheme, in order to make its runtime clinically relevant for the purpose of computerized planning of cryosurgery (Tanaka *et al* 2006). Verification of the uniform grid numerical scheme presented by Rabin and Shitzer (1998) is the objective of the current study, by comparison with experimental data. Since this comparison is performed on gelatin, the blood perfusion term and metabolic heat generation are set to zero in the current study. Note that heating due to blood perfusion during cryosurgery is a second-order effect and metabolic heat generation is negligible (Rabin and Shitzer 1998). While the blood perfusion rate and metabolic heat generation are set to zero for the purpose of the current study, the numerical scheme presented above accounts for these parameters. Further note that the stability of the numerical scheme increases with the increasing value of the blood perfusion term, while the metabolic heat generation bears no effect on stability (Rabin and Shitzer 1998). While comparison of the earlier version of the same scheme has been performed with experimental cryosurgery data (on an *in vivo* model of the rabbit hind thigh (Rabin *et al* 1996)), the accuracy of that comparison has not been established due to uncertainty in thermophysical properties of the relevant tissues; in turn, parametric estimation has been conducted there, in order to find the best-fit thermophysical properties. Further discussion with regard to the propagation of uncertainty in the thermophysical properties into heat transfer simulations and its application to cryobiology is discussed by Rabin (2003). The current study is performed on pure water, with well-documented physical properties, to a high degree of certainty, as listed in table 1.

While water—as a pure material—freezes at a unique temperature, biological tissues freeze over a wide temperature range, and the numerical technique has been developed accordingly. The numerical technique is based on the enthalpy approach, where an effective specific heat is defined so that the integral of the effective specific heat over some specific temperature interval is identical to the integral of the intrinsic specific heat over the same temperature interval, plus the latent heat. In a mixture, this interval is the phase transition temperature range (Rabin and Shitzer 1998); the range $-22\text{ }^{\circ}\text{C}$ to $0\text{ }^{\circ}\text{C}$ if the biological tissue is first-order approximated as an NaCl solution. It has been shown, however, that a pseudo-temperature range can also be assumed for the case of a pure material (Rabin and Korin 1993), without compromising the accuracy of the solution outside that temperature

range, while accurately accounting for the propagation of the freezing front. Following this approach, a pseudo-phase-transition temperature range of $-2\text{ }^{\circ}\text{C}$ to $+2\text{ }^{\circ}\text{C}$ is assumed for pure water in the current study.

Finally, it is noted that the freezing front location is interpolated from the temperature field, and it is not a solution parameter. It follows that, while the isotherm representing the freezing front is addressed in the current report, a clinician may wish to also present the location of any other isotherm, with the so called lethal temperature (frequently considered to be $-45\text{ }^{\circ}\text{C}$) as an example.

5. Comparison of experimental data with numerical results

Comparison between experimental data and numerical results in the current study includes the evolution of the frozen region volume and its shape, and the thermal history at pre-selected points. Since the heat transfer process is essentially 2D, a representative frozen region area is selected for this comparison, perpendicular to the axial direction of the cryoprobes. For this purpose, and consistent with prior work (Lung *et al* 2004, Rabin *et al* 2004, Rossi *et al* 2007, Tanaka *et al* 2006), a defect is defined as the difference in the frozen region area between experimental data and simulated results:

$$G = \frac{1}{A_E} \int_{A_s} w \, dA_s; \quad w = \begin{cases} 1 & -2\text{ }^{\circ}\text{C} < T_s & \text{interior to the experimental frozen region} \\ 0 & T_s \leq -2\text{ }^{\circ}\text{C} & \text{interior to the experimental frozen region} \\ 1 & T_s \leq -2\text{ }^{\circ}\text{C} & \text{exterior to the experimental frozen region} \\ 0 & -2\text{ }^{\circ}\text{C} < T_s & \text{exterior to the experimental frozen region} \end{cases} \quad (4)$$

where A_s is the area of the simulated domain, A_E is the area of the reconstructed frozen region from video recordings, and w is a weight function, dependent on the simulated temperature field, T_s . The temperature isotherm of $-2\text{ }^{\circ}\text{C}$ was selected for comparison purposes with the numerical simulation since it is the lower boundary of the pseudo-phase-transition range, and it corresponds to the complete release of the latent heat (i.e., completion of phase transition).

In order to compare the simulated frozen region contour with the experimental data, several measures have been taken. First, the pixel locations of each cryoprobe and the cryoheater were manually determined, with respect to the white corner dots, figure 3(a). Next, the white dots were registered relative to the numerical grid and each cryoprobe was relocated (snapped) to the closest numerical grid point. Since the numerical grid interval used in the current study is 0.5 mm, this relocation resulted in an uncertainty of 0.25 mm in the cryoprobe location. Finally, using a bilinear interpolation, results of the numerical simulation were interpolated into the image pixel grid, for the evaluation of equation (4) and the graphical presentation of temperature isotherms on experimental results. The average pixel size is 0.28 mm, where one half of it can be taken as a representative value of uncertainty in transformation between the numerical grids and the pixel grid.

Initial and boundary conditions for the numerical simulation were taken from experimental data, where the unique thermal history of each cryoprobe was taken into account, as well as the actual thermal history of the cryoheater. Consistent with the assumption of a 2D heat transfer process in the current study, the outer surfaces of both the cryoprobes and the cryoheater were taken to be uniform in the axial direction. A standard domain area of 130 mm \times 130 mm was applied to all numerical simulations. Consistent with experimental conditions, and prior discussion about boundary conditions (Rossi *et al* 2007), these domain dimensions are deemed large enough to be considered infinite (in x - y plane, perpendicular to the cryoprobe centerlines) for heat transfer considerations.

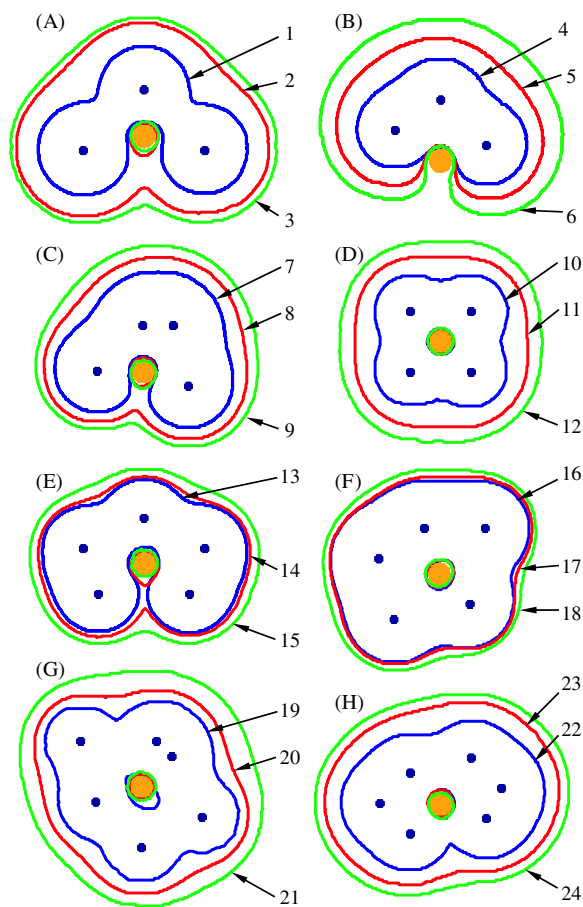


Figure 4. Eight cryoprobe layouts tested in the current study, where the freezing front is illustrated for each experiment at the point in time listed in table 2.

In addition, two hypodermic-needle thermocouples (type T, 1.5 mm OD) were strategically placed in the freezing region in each experiment, to measure the thermal history at specific locations and compare with simulated results. These thermocouples are identical to the one typically used during prostate cryosurgery (frequently placed between the prostate and the rectum).

6. Results and discussion

A total of 24 experiments were performed in this study, in eight representative cryoprobe layouts (figure 4); three experiments were repeated on each layout. For the purpose of the current discussion, one point in time was selected for each experiment for comparison between experimental data and numerical simulation, as listed in table 2. The freezing front location for each experiment, at the specific point in time listed in table 2, is also illustrated in figure 4.

Table 2. Summary of experimental data and numerical results, where n is the number of cryoprobes, t_C is the time at which the comparison is performed, A_E is the reconstructed area of the frozen region, A_S is the simulated area of the frozen region (below $-2\text{ }^\circ\text{C}$), D_I is the interior defect, D_E is the exterior defect, and ΔS is the average difference in freezing front location between the numerical solution and experimental data; the various layouts are displayed in figure 4.

No.	Layout	n	t_C (min)	A_E (mm ²)	A_S (mm ²)	Defect (%)	D_I (mm ²)	D_E (mm ²)	ΔS (mm)
1	A	3	10	2008	1980	4.7	61.4	33.5	0.39
2	A	3	22	3838	3943	3.0	3.4	111.4	0.49
3	A	3	29	4431	4551	2.9	1.4	126.1	0.50
4	B	3	8	1531	1509	3.5	38.2	15.1	0.36
5	B	3	16	2572	2574	3.9	45.5	54.7	0.51
6	B	3	27	3814	3993	4.7	0.1	178.7	0.79
7	C	4	9	2091	2100	3.3	30.3	37.8	0.36
8	C	4	14	2961	2983	1.9	15.6	40.6	0.28
9	C	4	19	3658	3723	2.1	3.4	73.1	0.35
10	D	4	7	1624	1601	3.2	38.7	13.9	0.28
11	D	4	13	2718	2759	2.8	16.3	58.8	0.40
12	D	4	20	3627	3762	3.9	0.1	142.1	0.63
13	E	5	8	2451	2464	4.3	46.7	59.0	0.41
14	E	5	9	2760	2782	2.8	26.3	49.7	0.30
15	E	5	12	3392	3483	3.1	6.6	98.7	0.47
16	F	5	10	3019	3023	1.9	25.3	32.4	0.23
17	F	5	11	3168	3203	1.9	12.0	47.7	0.25
18	F	5	13	3606	3617	1.5	23.2	32.3	0.26
19	G	6	7	2570	2545	3.7	61.2	34.4	0.35
20	G	6	13	3531	3570	1.5	6.9	44.7	0.22
21	G	6	17	4769	4851	2.1	7.3	91.0	0.45
22	H	6	7	2389	2395	2.7	28.3	36.9	0.30
23	H	6	12	3544	3604	2.1	6.7	66.2	0.35
24	H	6	16	4297	4431	3.2	0.3	135.2	0.53

For demonstration purposes, figure 5 displays predictions of the freezing front location (dotted line), superimposed on the respective images taken from experiment #22 on cryoprobe layout H, at four different points in time. It can be seen from table 2 that the per cent defect, equation (4), between experimental data and the numerical simulation at 7 min is 2.7% for this case. Defect values listed in table 2 are less than 5%, with an average value of 2.9%.

In addition to the defect calculation, an average uncertainty in the simulated freezing front location is calculated, by dividing the absolute defect by the perimeter of the frozen region. In experiment #22 for example, the absolute defect is found by adding the interior and exterior defects, 28.3 mm² and 36.9 mm², respectively (table 2). The frozen region perimeter (i.e., the freezing front length) at this time is 215 mm (not listed in table 2). Thus, there is an uncertainty of 0.3 mm in freezing front location (table 2). The most significant factors affecting this uncertainty are: (1) uncertainty of 0.25 mm due to cryoprobe relocation, when identifying its location on the numerical grid (see section 5)—parametric studies showed that this effect alone can lead to a defect area of about 1.5%; (2) uncertainty of 0.13 mm due to bilinear interpolation of temperature data from the numerical grid to the image-pixel grid (see section 5); (3) uncertainty in temperature measurement of the cryoprobe, in the range of 0.5 °C; (4) non-uniform temperature distribution in the cryoprobe cross-section, which can lead to up to a few centigrade degrees, depending on the liquid nitrogen boiling regime, and therefore on the cryoprobe temperature; (5) uncertainty due to the pseudo-phase-transition temperature range

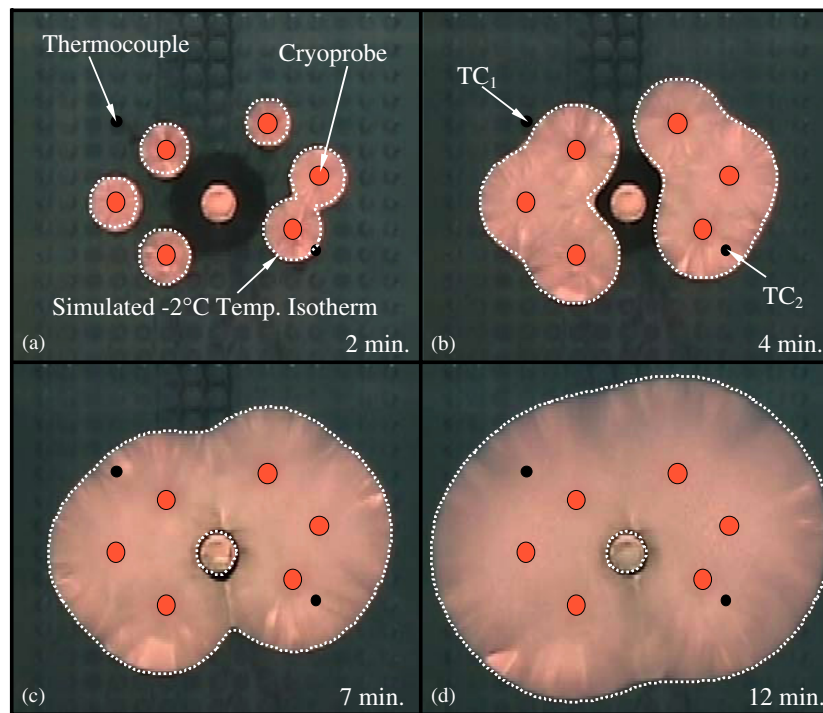


Figure 5. Snap-shots of the frozen region at four representative points in time (experiment 22, table 2), with the simulated freezing front superimposed (dotted line).

for pure water of ± 2 °C; (6) uncertainty in thermophysical properties of water, and especially at low cryogenic temperatures (Rabin 2003); (7) uncertainty associated with segmentation (see section 3); and (8) heat gain from the surroundings through the Plexiglas walls of the container—and thereby deviation of the heat transfer problem from 2D—estimated as 2% of the total heat transfer in the system, based on simulation of conduction through the Plexiglas wall and free convection to the surroundings (note that thermal conductivity of the Plexiglas is less than 4% of that of ice upon freezing, a ratio which increases with decreased temperature). Given all the parameters contributing to uncertainty in estimation of the freezing front location, the average disagreement of 0.3 mm between experimental data and numerical simulation is deemed an excellent outcome in the current study.

Defect values listed in table 2 provide a comparison between experimental data and simulation results at single points in time. Figure 6 displays the evolution of uncertainty in freezing front location with time, for four representative cases. It can be seen from figure 6 that the uncertainty in the freezing front location remains below 0.6 mm with time, with an average value of about 0.4 mm, for the cases shown; a similar trend was found in other experiments.

Figure 7 displays the measured thermal history at two points in the domain of experiment #22 (illustrated in figure 5), and the corresponding simulation results. The small temperature fluctuations in the simulated results correspond to fluctuations in cryoprobe temperatures, as a result of the on-off control of the cryoprobes and the two-phase flow (nitrogen liquid and vapors) in the cryoprobes. Although a similar trend is observed in the experimental data, the magnitude of the corresponding fluctuations in the experimental data is smaller, due to the time

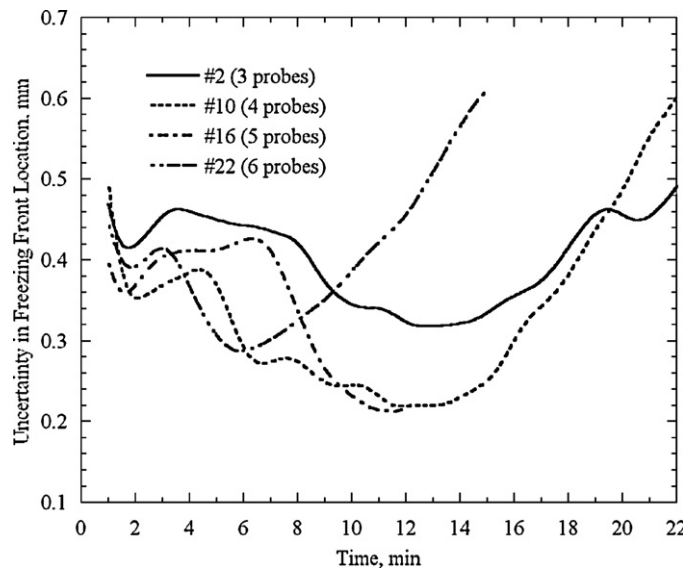


Figure 6. Uncertainty in the freezing front location, comparing experimental data with simulation results, for four representative experiments listed in table 2.

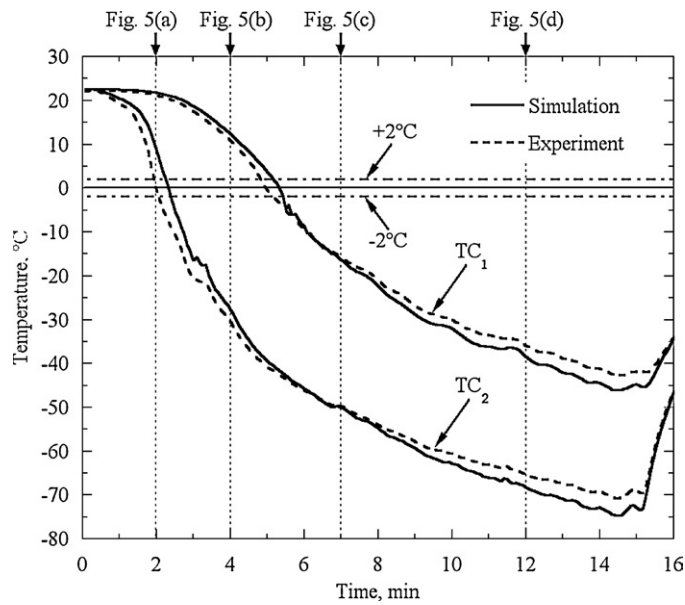


Figure 7. Thermal histories at the thermocouple locations, TC_1 and TC_2 , in experiment #22 (figure 5).

response of the hypodermic thermocouple (embedded in a 1.5 mm in diameter stainless-steel tube). The average difference between the predicted and measured thermal histories is 2.1 °C. Note that the time points at which results are displayed in figure 5 are also marked on figure 7. It can be seen from figure 7 that the temperature difference between simulation results and experimental data, when the thermocouples indicate 0 °C, is 4 °C and 8 °C,

for TC_1 and TC_2 , respectively. These temperature differences far exceed the ± 2 °C range defining the pseudo-phase-transition temperature range, which suggests that other effects are also contributing significantly to this difference. Similar results were obtained for the other experiments, with various thermocouple locations.

Runtime for the 2D simulations performed in the current study, using a uniform grid size, was up to 10 min on a 3.4 GHz Pentium 4 machine, with 512 MB of memory, and 800 MHz front side bus. When optimizing the numerical scheme for variable grid size and time intervals, as demonstrated by Rossi *et al* (2007), complete 3D simulations with similar parameters are executed in less than 2 min, with a similar degree of numerical accuracy, where the uniform grid results serve as a benchmark. For clinical planning using the so-called bubble-packing technique (Tanaka *et al* 2006), only a single bioheat transfer simulation would be required, where bubble-packing runtime is measured in seconds. For a more accurate planning process, using a two-phase planning scheme of bubble packing followed by the so-called force-field method, a few repeated heat transfer simulations would be required, leading to a full-scale planning in under 10 min (Tanaka *et al* 2006).

The discussion now turns to the application of the numerical technique for computerized planning of cryosurgery. The typical resolution of ultrasound imaging, during prostate cryosurgery (Tanaka *et al* 2007), is typically not better than 1 mm. Uncertainty in estimating the freezing front location, based on ultrasound imaging, can easily exceed this 1 mm threshold, if additional parameters such as ultrasound hardware and software, and variance in tissue properties are considered. It follows that uncertainty in estimating the freezing front location in the current study, based on heat transfer simulations, is smaller than the uncertainty in estimating the freezing front location based on ultrasound imaging, in a clinical setup. Furthermore, given the quality of agreement between experimental data and numerical simulations presented in the current study, the typical quality of organ reconstruction for cryosurgery applications, and the fact that the defect area concept is the key for computerized planning in parallel studies (Lung *et al* 2004, Rabin *et al* 2004, Tanaka *et al* 2006), it is concluded that the numerical technique presented by Rossi *et al* (2007) is adequate for the purpose of computerized planning of cryosurgery using the prototype algorithms presented by Lung *et al* (2004), Rabin *et al* (2004) and Tanaka *et al* (2006).

For the purpose of computerized planning of cryosurgery, the actual properties of the specific tissues must be taken into account. Selected thermophysical properties of biological materials are widely available in the literature (for example, Chato (1985)), while planning for a specific organ may require further measurements of thermophysical properties. However, before one attempts to measure thermophysical properties of a specific tissue to a higher degree of certainty, it is highly recommended that the effect of the available level of uncertainty in property values on the estimation of the freezing front location be assessed, as demonstrated by Rabin (2003). If the resulting uncertainty in freezing front location is not worse than the uncertainty in organ reconstruction, organ imaging and/or freezing front imaging—all of which may be quite significant—then further investigation of thermophysical properties for that clinical application is not warranted. In this context, it is reminded that the numerical scheme is used from computerized planning only, and not as a substitute to real time monitoring.

7. Summary and conclusions

The current study is focused on experimental verification of a numerical scheme applied for computerized planning of cryosurgery. A new experimental apparatus has been developed for this purpose, leading to a 2D heat transfer process, simulating a cross section of the prostate

during cryosurgery. A new technique for analysis of the frozen region shape, from video recordings, has also been presented.

A total of 24 experiments were performed in this study, in eight representative cryoprobe layouts; three experiments were repeated on each layout. Results indicate defect areas of less than 5%, with an average value of 2.9%, between experimental data and simulation results. Results further indicate an average uncertainty of 0.4 mm in freezing front location.

Uncertainty of not less than 1 mm in identifying the prostate contour is probably a lower boundary, when using a single rectal ultrasound transducer during prostate cryosurgery. In fact, due to the typical quality of ultrasound imaging, some surface areas of the organ are interpolated based on imaging data, rather than directly extracted from imaging. Given the quality of agreement between experimental data and numerical simulations presented in the current study, the typical quality of organ reconstruction for cryosurgery applications, and the fact that the defect area concept is the key for computerized planning in parallel studies, it is concluded that the numerical technique presented by Rossi *et al* (2007) is adequate for the purpose of computerized planning of prostate cryosurgery using the prototype algorithms presented by Lung *et al* (2004), Rabin *et al* (2004) and Tanaka *et al* (2006).

Acknowledgments

This project is supported by the National Institute of Biomedical Imaging and Bioengineering (NIBIB)—NIH, grant #R01-EB003563-01,02,03,04. The authors would like to thank Mr Jim Dillinger, Mr John Fulmer and Mr Edward Wojciechowski, of the Machine Shop, Department of Mechanical Engineering, Carnegie Mellon University, Pittsburgh, PA, for assistance and advice in constructing the experimental system.

References

- Baissalov R, Sandison G A, Reynolds D and Muldrew K 2001 Simultaneous optimization of cryoprobe placement and thermal protocol for cryosurgery *Phys. Med. Biol.* **46** 1799–814
- Cengel Y A and Boles M A 2002 *Thermodynamics: An Engineering Approach* (New York: McGraw-Hill)
- Chang Y L and Li X B 1994 Adaptive image region-growing *IEEE Trans. Image Process.* **3** 868–72
- Chato J C 1985 Selected thermophysical properties of biological materials *Heat Transfer in Biology and Medicine* ed A Shitzer and R C Eberhart (New York: Plenum) pp 413–8
- Cooper I S and Lee A 1961 Cryostatic congelation: a system for producing a limited controlled region of cooling or freezing of biological tissues *J. Nerve Mental Dis.* **133** 259–63
- Diller K R 1992 Modeling of bioheat transfer processes at high and low temperatures *Advances in Heat Transfer* ed J P Hartnett, T F Irvine and Y I Cho (New York: Academic) pp 157–358
- Gage A A 1992 Cryosurgery in the treatment of cancer *Surg. Gynecol. Obstetric.* **174** 73–92
- Gage A A and Baust J 1998 Mechanisms of tissue injury in cryosurgery *Cryobiology* **37** 171–86
- Gilbert J C, Rubinsky B, Wong S, Pease G R, Leung P P and Brennan K M 1997 Temperature determination in the frozen region during cryosurgery of rabbit liver using MR image analysis *Magn. Res. Imaging* **15** 657–67
- Holman J P 2002 *Heat Transfer* (New York: McGraw-Hill)
- Keanini R G and Rubinsky B 1992 Optimization of multiprobe cryosurgery *ASME Trans. J. Heat Transfer* **114** 796–802
- Lung D C, Stahovich T F and Rabin Y 2004 Computerized planning for multiprobe cryosurgery using a force-field analogy *Comput. Methods Biomech. Biomed. Eng.* **7** 101–10
- Onik G M, Cohen J K, Reyes G D, Rubinsky B, Chang Z H and Baust J 1993 Transrectal ultrasound-guided percutaneous radical cryosurgical ablation of the prostate *Cancer* **72** 1291–99
- Onik G M, Gilbert J C, Hoddick W, Filly R, Callen P, Rubinsky B and Farrel L 1985 Sonographic monitoring of hepatic cryosurgery in an experimental animal model *Am. J. Roentgenol.* **144** 1043–47
- Pennes H H 1948 Analysis of tissue and arterial blood temperatures in the resting human forearm *J. Appl. Phys.* **1** 93–122

- Pohle R and Toennies K 2001 Segmentation of medical images using adaptive region growing *Proc. SPIE Medical Imaging (San Diego, CA)* vol 4322 (Bellingham, WA: SPIE Press) pp 1337–46
- Rabin Y 1998 Uncertainty in temperature measurements during cryosurgery *Cryo-Letters* **19** 213–24
- Rabin Y 2003 A general model for the propagation of uncertainty in measurements into heat transfer simulations and its application to cryobiology *Cryobiology* **46** 109–20
- Rabin Y, Coleman R, Mordohovich D, Ber R and Shitzer A 1996 A new cryosurgical device for controlled freezing, part II: *in vivo* experiments on rabbits' hind thighs *Cryobiology* **33** 93–105
- Rabin Y, Julian T B and Wolmark N 1997 A compact cryosurgical apparatus for minimal-invasive cryosurgery *Biomed. Instrum. Technol.* **31** 251–8
- Rabin Y, Julian T B and Wolmark N 1999 Method and apparatus for heating during cryosurgery *US Patent No.* 5,899,897
- Rabin Y, Julian T B and Wolmark N 2000 Method and apparatus for minimal-invasive cryosurgery *US Patent No.* 6,039,730
- Rabin Y and Korin E 1993 An efficient numerical solution for the multidimensional solidification (or melting) problem using a microcomputer *Int. J. Heat Mass Transfer* **36** 673–83
- Rabin Y, Lung D C and Stahovich T F 2004 Computerized planning of cryosurgery using cryoprobes and cryoheaters *Technol. Cancer Res. Treatment* **3** 227–43
- Rabin Y and Shitzer A 1998 Numerical solution of the multidimensional freezing problem during cryosurgery *ASME J. Biomech. Eng.* **120** 32–7
- Rabin Y and Stahovich T F 2003 Cryoheater as a means of cryosurgery control *Phys. Med. Biol.* **48** 619–32
- Rossi M R, Tanaka D, Shimada K and Rabin Y 2007 An efficient numerical technique for bioheat simulations and its application to computerized cryosurgery planning *Comput. Methods Programs Biomed.* **85** 41–50
- Rubinsky B, Gilbert J C, Onik G M, Roos M S, Wong S T S and Brennan K M 1993 Monitoring cryosurgery in the brain and the prostate with proton NMR *Cryobiology* **30** 191–99
- Schulz T, Puccini S, Schneider J P and Kahn T 2004 Interventional and intraoperative MR: review and update of techniques and clinical experience *Eur. Radiol.* **14** 2212–27
- Serra J 1982 *Image Analysis and Mathematical Morphology* (London: Academic)
- Tanaka D, Rossi M R, Shimada K and Rabin Y 2007 Towards intra-operative computerized planning of prostate cryosurgery *Int. J. Med. Robot. Comput. Assisted Surg.* **3** 10–9
- Tanaka D, Shimada K and Rabin Y 2006 Two-phase computerized planning of cryosurgery using bubble-packing and force-field analogy *ASME J. Biomech. Eng.* **128** 49–58
- Turk T M T, Rees M A, Myers C E, Mills S E and Gillenwater J Y 1999 Determination of optimal freezing parameters of human prostate cancer in a nude mouse model *Prostate* **38** 137–43